[American Journal of Science, Vol. 307, March, 2007, P. 590–611, DOI 10.2475/03.2007.02]

GALENA STABILITY TO 26 KBAR

KEVIN T. WHEELER*, DAVID WALKER*, and MARIE C. JOHNSON**

ABSTRACT. The melting point of galena was measured by differential thermal analysis to 25 kbar. The melting point is 1191 °C at 5.9 kbar and increases to ~1315 °C by 25 kbar along a concave-down trajectory. The form of the PbS melting curve resembles those of similarly structured compounds that show a range of initial slopes and curvatures. Initial liquidus slopes of several B1-structured compounds including PbS correlate well with melting volume change. However, the roughly 25 J/mol*K entropy of melting required for PbS by the volume of melting, initial liquidus slope, and Clapeyron equation is approximately double literature estimates. Similar discrepancies exist for the other B1-structured compounds. Liquidus curvature correlates well with the initial ratio of liquid to solid compressibility. PbS liquid compressibility of ~$12*10^{-12}$ cm^2/ dyne is estimated from galena compressibility and initial melting slope. The transformation of galena from cubic to orthorhombic structure with pressure was determined by electrical resistance measurements up to 1000 °C and occurs at about 26 kbar with little temperature variation. Galena's maximum stability is at the inferred triple point among galena, liquid, and orthorhombic-structured PbS at ~26 kbar and ~1315 °C.

INTRODUCTION

Galena (PbS) is the world's most abundant Pb mineral, is the fourth most abundant sulfide, and is commonly found in sedimentary, metamorphic and igneous rocks. Geochemists routinely use galena for Pb-Pb dating because of its high concentration of Pb relative to U, Sb, Bi, and Ag are frequently associated with galena as either trace constituents or accessory mineral phases.

NaCl-structured PbS melts at approximately 1115 °C at one atmosphere. This melting point is substantially higher than the melting points of monosulfides HgS (580°C), SnS (880°C) and NiS (976°C), somewhat less than FeS (1188°C), and significantly less than ZnS (1700°C) (table 1). A study by Sharp (1969) employed a belt apparatus and quenching techniques to identify the melting curves of ZnS, PbS, and FeS from 30 to 65 kbars. The methods he used, however, were not sufficiently precise to resolve the melting curves with great certainty. Extensive follow up work has been done on the FeS system by Ryzhenko and Kennedy (1973), Williams and Jeanloz (1990), Boehler (1992), and Kavner and others (2001). The other monosulfides, however, have not attracted as much attention, and their melting curves in pressure-temperature space have not been reliably determined.

Many studies have investigated the melting point of PbS at one atmosphere. Friedrich and Leroux (1905) found the melting point to be 1103°C, Friedrich (1907a, Friedrich, 1907b) 1114°C, Blitz (1908) 1112°C ± 2°C, Truthe (1912) and Heike (1912) 1106°C, Van Hook (1960) 1115°C ± 5°C, and Kullerud (1969) 1115°C. Bloem and Kröger (1956) found that slightly greater than stoichiometric Pb (0.03 atomic percent) increases the melting point 50°C from 1077°C for PbS to 1127°C for $PbS_{0.9997}$.

A first order phase transition from a cubic NaCl structure to an orthorhombic SnS-like structure in PbS has been reported to occur at approximately 25 kbar at room temperature Bridgman (1940), Takahashi and others (1964), Mariano and Chopra (1967), Wakabayashi and others (1968). In all studies, the phase boundary is not

*Lamont Doherty Earth Observatory and Department of Earth and Environmental Sciences, Columbia University, Palisades, New York 10964 USA; kwheeler@ldeo.columbia.edu; dwalker@ldeo.columbia.edu

**Department of Geography and Environmental Engineering, U S Military Academy, West Point, New York 10996

Table 1

Crystal information

Compound	Crystal System	Structure Type	a	b	c	Bond Length Å	T_m °C	Ref.
PbS	cubic	NaCl (B1)	5.936			2.968	~1115	1,2
AgCl	cubic	NaCl	5.547			2.774	~450	1,2
AgBr	cubic	NaCl	5.775			2.887	~430	1,2
KCl	cubic	NaCl	6.293			3.146	~775	1,2
NaBr	cubic	NaCl	5.974			2.987	~740	1,2
SnS*	orthorhom.	SnS	4.330	11.180	3.980	2.165	880	1,2
HgS*	cubic	ZnS	5.858			2.929	580	1,2
ZnS	cubic	NaCl	5.406			2.703	1700	1,2
NiS*	hexagonal	NiAs	3.428		5.340	1.714	976	1,2
FeS	hexagonal	Troilite	5.946		11.720	2.973	1188	1,2

*To our knowledge, no data have been published on the high pressure melting relations of these compounds. [1]Donnay and Ondik (1973). [2]Winter (2006).

sharply defined. It has been suggested that this lack of precision is caused by the sluggishness of the transformation.

This study explores the melting point of PbS up to 25 kbar. The shape and slope of the PbS melting curve are compared to those of similarly sized and structured compounds (AgCl, AgBr, KCl, NaBr) as well as monosulfide FeS. The inversion to the denser orthorhombic structure is also explored as a function of temperature.

Experimental methods for galena melting study

Starting Material

200 mesh Lead(II) Sulfide powder of 99.9+ percent purity purchased from Aldrich Chemical Company was used for the melting experiments described here. A stainless steel die with a tungsten carbide rod was used to compact the PbS powder into cylinders prior to placement in the sample assembly.

Sample Assembly

A COMBAT boron nitride (BN) grade HP capsule was used to contain the PbS cylinder (fig. 1). Low molten viscosity and disposition to react with many commonly used capsule materials make PbS difficult to contain. Grade HP BN, while imperfect, provided the best container for PbS of any tested. Fractures that developed upon pressurization provided conduits for minor PbS mobilization and potential loss at experimental conditions. However, its low porosity, good thermal conductivity, resistance to wetting by metals and relative chemical inertness in the presence of PbS made it the favored choice in this study.

A hole of the same dimensions as the PbS cylinder was drilled into the BN. The PbS cylinder was placed inside, and a BN end cap was used to complete the container. A graphite heater surrounded the BN capsule, end cap and upper and lower magnesium oxide (MgO) spacers. A thin-wall barium carbonate ($BaCO_3$) hollow cylinder fitted around the graphite heater and served as the confining pressure medium. The thin wall $BaCO_3$ was wrapped in lead foil before being placed on top of a graphite disc inside a 1/2 inch inner diameter pressure vessel of a Boyd-England-style piston cylinder apparatus. A steel base plug with a pyrophyllite sleeve provided electrical contact between the graphite heater and overlying pressure plate.

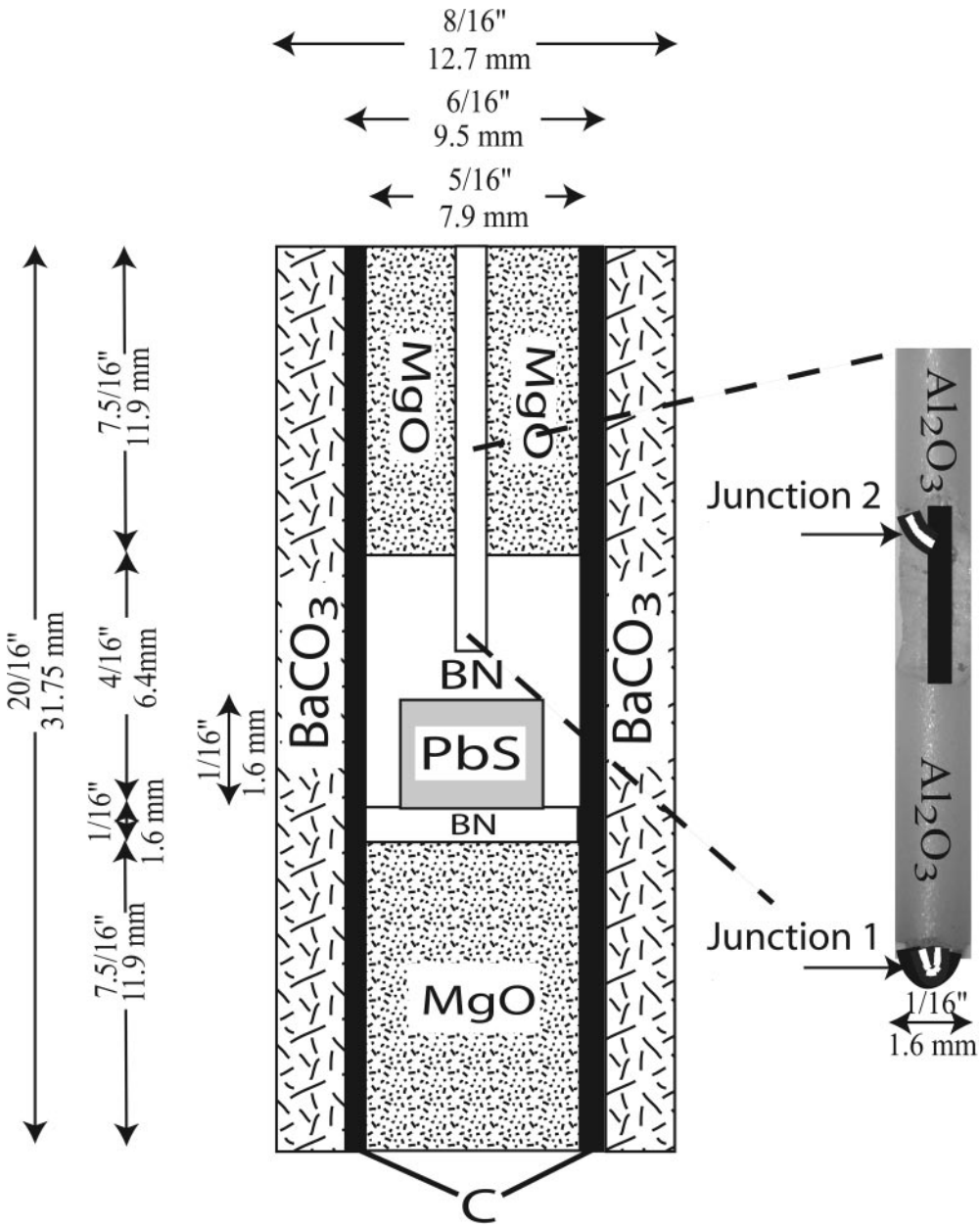

Fig. 1. Sample assembly. Grade HP Combat® Boron Nitride (BN) capsule is used to contain the Lead Sulfide (PbS). The thermocouple well is drilled into the BN capsule to improve the thermal signal received by the thermocouple. The double junction three wire DTA thermocouple is seen in the cutout. One negative lead of W 97 Re 3 thermocouple wire (black line) makes contact with two positive leads of W 75 Re 25 wire (white line). Junction 1 is at the end of the Al_2O_3 thermocouple tubing and is closest to the PbS charge and thermal hotspot. Junction 2 is farther away from the hotspot and PbS charge and is less affected by the heat of freezing of the PbS. The difference in voltage (temperature) between the positive wires of junction 1 and the cooler junction 2 is what is plotted by the chart recorder (fig. 2).

Run Conditions

Typically, over the span of two hours, conditions in the pressure vessel were raised to 10kb and 800 °C. The run was then allowed to sinter for at least 12 hours before the differential thermal analysis (DTA) was performed. Over the course of a DTA experiment, samples experienced pressures ranging from 5 to 26 kbar and maximum temperatures reaching 1345 °C.

Differential Thermal Analysis

DTA, as applied in this study, made use of the enthalpy of freezing to detect the freezing point of PbS. A Type D W-Re double junction, three wire thermocouple was used without correction for the effect of pressure (fig. 1). The junction at the end of the Al_2O_3 thermocouple tubing, junction 1, was closest to the assembly hotspot and the PbS charge. Junction 2 was located farther away from the hotspot and sample in a cooler region of the assembly.

The thermal gradient in the assembly caused the two thermocouple junctions to read different temperatures. The temperature difference between the two junctions was plotted on a Linseis L7005 chart recorder. When the temperature was manually lowered from a setting where it was higher than the melting point of PbS to a setting where it was lower, two signals appeared. First, the differential temperature plot showed lower values because of a shallower thermal gradient. Second, this effect was briefly counteracted by release of the PbS enthalpy of freezing. The heat given off by the PbS freezing affected junction 1 most, causing it to experience a less rapid temperature drop. The result was a brief increase in the differential that manifested itself as a bump on the otherwise smoothly decreasing signal on the chart recorder.

At a constant pressure, the temperature of a run was typically raised to a set-point, held for several minutes to stabilize, and then dropped while the differential signal was monitored on the chart recorder. If a signal indicating PbS freezing was observed during the drop, the temperature was raised back to a slightly lower level, held, and then dropped again while looking for a signal. This process was repeated at successively lower temperatures until no freezing signal was observed. The melting point of the PbS was interpreted to lie below the lowest temperature drop with a signal and above the highest temperature drop with no signal, typically a 5°C range. Melting signals became increasingly faint and consequently difficult to detect at progressively higher pressures. The implications of this will be discussed in following sections. The details of the DTA procedure can be seen in figure 2.

Mounting and Polishing

Following an experiment, the assembly was quenched, depressurized and pressed out of the pressure vessel. The assembly was then impregnated with epoxy and placed on a hot plate for several hours until the epoxy cured. Assemblies were ground into with wet diamond-impregnated wheels and then polished on a succession of 240, 320, 400 and 600 silicon carbide papers. The final polishing was done with 0.3μ alumina grit. A typical finished product can be seen in figure 3.

Microprobe Analysis

To determine the stoichiometric variability of Pb and S in the experimental charge, samples were analyzed using the Lamont-Doherty CAMECA electron microprobe at a 25kV gun voltage and a 10nA beam current in raster mode with $10\mu^2$–$30\mu^2$ fields of view. Pb was analyzed using its Lα line and S was analyzed using its Kα line. Both elements had +/− 600 spectrometer steps off peak to correct for background. A galena standard was used to standardize both Pb and S.

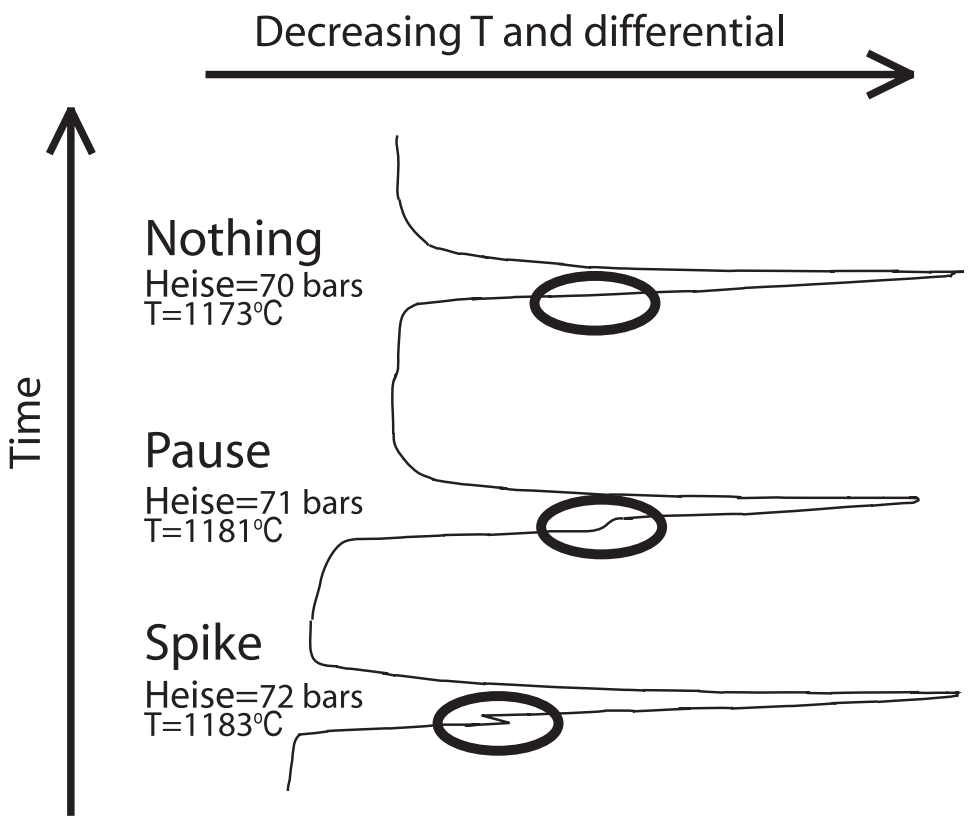

Fig. 2. Representative plot of a DTA chart recorder output logging the differential signal from the thermocouple. All three types of signal (spike, pause, nothing) are shown. The temperature started at 1183°C and was then dropped to an arbitrary value several hundred degrees below. Since 1183°C was above the melting point of PbS at 5.9 Kbar, a prominent spike develops on the slope of the decreasing differential. The temperature was then raised to 1181°C and dropped again. The falling differential pauses slightly as the PbS freezes, producing a gentle bulge in the curve. Finally, the temperature is raised to 1173°C and dropped producing no signal. This indicates that 1173°C is below the melting point of PbS at 5.9Kbar. The melting point is taken as 1177°C at this pressure, the midpoint between the lowest temperature drop with a freezing signal and the highest temperature drop without a signal.

Pressure Calibration

The melting point of Au was used to calibrate pressure in the thin wall $BaCO_3$ assemblies (fig. 4). The melting point was measured by DTA at pressures ranging from 100 to 200 bars of oil pressure. Melting points at their respective oil pressures were then correlated with the Au melting curve of Akella and Kennedy (1971) to obtain the true pressures of melting. Actual pressures per unit of oil pressure in the assemblies were lower than would occur in a frictionless environment but higher than would be observed with thick $BaCO_3$. This difference indicates unsurprisingly that less frictional resistance occurs in the thin wall assemblies than in the thick. Pressure corrections for friction with thin wall $BaCO_3$ assemblies were calculated from:

$$P\ \text{kbar} = 0.0959 * (\text{oil pressure bars}) - 0.8243 \quad (1)$$

RESULTS— GALENA MELTING STUDY

Figure 5 shows data from experiment GG867, the most reliable of three apparently successful runs. All three runs had identically shaped melting curves that were

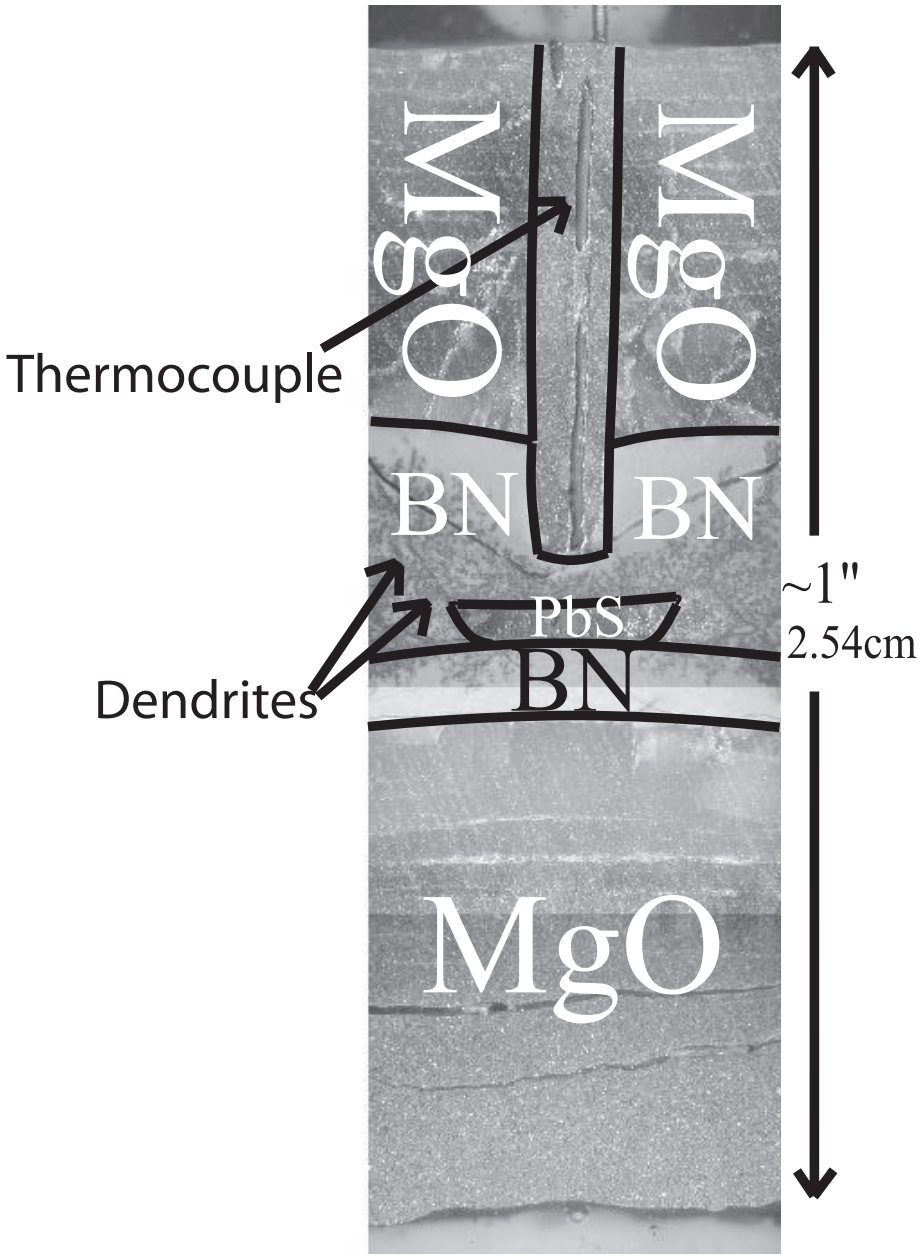

Fig. 3. Image of experiment GG861 after being run, mounted and polished. Some PbS has leaked out into the BN causing dendrites and into the MgO causing discoloration. The majority of PbS, however, remained in its original location. The BN experienced some fracturing which may have facilitated PbS escape and dendrite formation. The thermocouple remained segregated enough from the PbS as not to have caused failure. The assembly as a whole appears slightly deformed but essentially intact.

offset from each other by 20 to 100 °C. GG867 was deemed most reliable because optical and chemical assessments revealed no signs of thermocouple or BN contamination as were observed or inferred in the other runs. An experiment with the thermo-

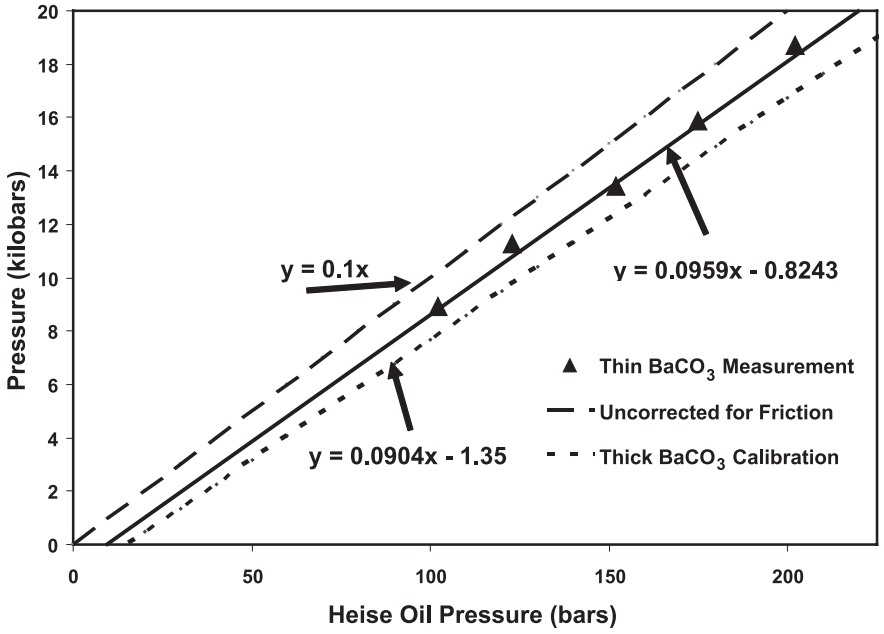

Fig. 4. Plot of oil pressure versus kbar for the thin-wall $BaCO_3$ piston cylinder assembly. The frictionless pressure relationship has a slope of 0.1 kbar/oil bar (black line) for a 5″ ram driving a 0.5″ piston. The melting point of Au was determined with DTA in the thin-wall $BaCO_3$ assembly from 100 to 200 Heise bars (triangles) and then compared to the Akella and Kennedy (1971) Au melting curve. The pressure calibration curve for a thick-wall $BaCO_3$ assembly (short dashed line) (Fram and Longhi, 1992) has a lower intercept than the thin-wall assembly consistent with less efficient pressure transmission (more friction).

couple in direct contact with the PbS (GG865) yielded a melting curve more than 60 °C below GG867 possibly due to freezing point depression from contamination by thermocouple material. The melting curve from the other run (GG861) was 20 °C lower than GG867. This difference could be due to its long run duration and possible sub-detection-limit B and/or N contamination in the PbS incurred over time, or slight thermocouple degradation.

Microprobe analyses revealed, within analytical error, stoichiometric PbS for all measurements in the main region of the charge. Attempts to measure the composition of PbS in the dendrites were unsuccessful due to the small size of the dendrites.

PbS melting was presumed, for lack of evidence to the contrary, to be congruent at all pressures. This assumption is difficult to verify without *in situ* analyses because the liquid phase did not quench. We observed, as mentioned previously, a decrease in freezing signal intensity with increasing pressure, consistent with, but not confirming, a departure from congruent melting behavior with increasing pressure. However, there is no evidence to suggest peritectic melting, involving some unknown phase, or loop melting by a charge that has somehow wandered off composition and has evaded detection of its compositional degradation.

We specifically looked for B and N contamination in the quenched galena without result. Direct analysis for B and N is possible at the level of a few percent, and so differences from 100 percent for the sum of Pb and S provide a more sensitive test of contamination. None was found, nor were significant departures from PbS stoichiometry observed.

The melting points were calculated as the midpoints between the lowest temperature melting signals and the highest temperature no-signals at particular pressures.

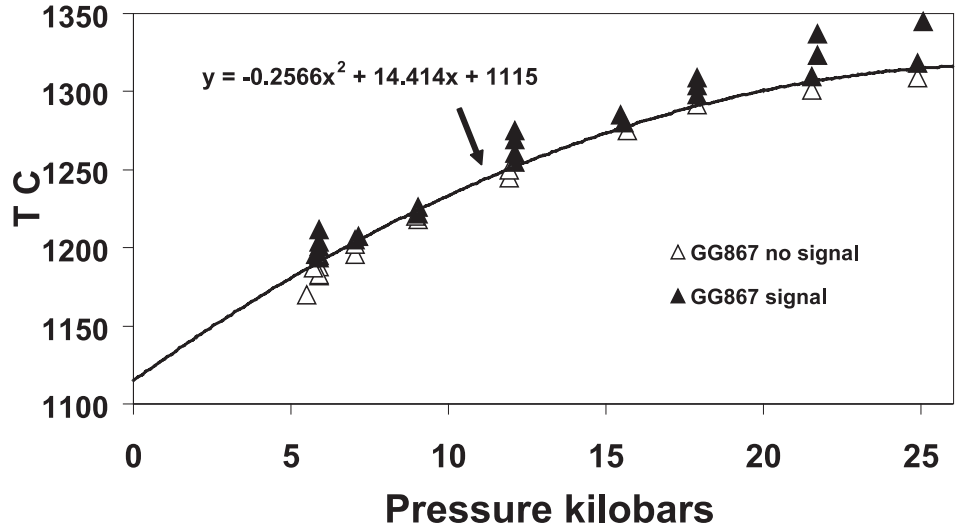

Fig. 5. Raw DTA data from GG867 and the calculated melting curve. Closed symbols represent spikes and pauses. Open symbols represent temperatures at which no signal was observed. GG867 was the experiment least affected by contamination and is therefore the most representative of the true melting behavior of PbS. The polynomial fits melting points calculated from the difference between the lowest temperature signal and highest temperature non-signal at a particular pressure.

The thick central line in figure 5 tracks temperature of melting for PbS as it increases gradually along a concave-down trajectory from 1191 °C at 5.9 kbar to ~1315 °C at almost 25 kbar. The data appear almost linear until about 18 kbar when the liquidus unequivocally flattens out. A second order polynomial best fits the combination of this study's and published one atmosphere data:

$$T_m = -0.2566 * P^2 + 14.414 * P + 1115 \quad (2)$$

Where T_m is in °C and P is kbar.

This flattening, if not an experimental artifact, resembles the flattening shown by alkali halide melting curves in the vicinity of inversions of the solid phase to higher-density polymorphs. Liquidus flattening, or "droop," has been observed in numerous materials and is typically attributed to greater compressibility in the liquid than in the solid. Pistorious (1965) made the observation that this tendency towards flattening increases systematically with anion size for the potassium halides. Walker and others (2002) proposed that effects like these systematics arise through weakening of bonding in both the higher density and larger anion forms of these compounds. Liquidus "droop" approaching the triple point between B1, B2, and liquid KCl was analyzed in the context of new determinations of the thermal equations of state of B1 and B2 KCl. Surprisingly the high density solid, B2 KCl, has a substantially larger thermal expansion than sylvite, B1 KCl. The increasing coordination number in high density forms reduces ionic polarization, leading to larger effective ion sizes. Thus the progression in polymorphic forms to higher coordination number parallels the progression seen from increasing anion size through chemical substitution. Larger effective ionic size reduces the electrostatic bond strength. Walker and others (2002) inadvertently rediscovered some of the conclusions of Jeanloz and Roufousse (1982) who reached their insights from different data and reasoning, without invoking the effects of ionic polarization that are central to the Walker and others (2002) interpretation of the KCl

and RbCl thermal equations of state. The convergence of both studies on the nature of the effects expected from a phase change to higher density makes the flattening of the PbS liquidus near the phase transition a plausible expectation. Because the background reference material, cited above, suggests the existence of a phase transition of galena to the higher-density orthorhombic structure in roughly the pressure range of the liquidus flattening, we explored the thermal variation of this solid-state phase transition. Does the cubic-orthorhombic structure solid-state phase transition intersect the liquidus for PbS in a manner consistent with the interpretation that the liquidus curvature is related to the approach to the invariant point? Or does it miss the liquidus?

Galena's cubic to orthorhombic structure transition

The collapse at ~25 kbar and room temperature of galena to a ~3 percent denser phase was reported by Bridgman (1940). Takahashi and others (1964), Mariano and Chopra (1967), and Wakabayashi and others (1968) identified the high pressure modification as an orthorhombic, SnS-type (B29) distorted rock salt structure. Others have identified the modification as other orthorhombic structures such as GeS (B16) by Chattopadhyay and others (1986) and CrB (B33) by Knorr and others (2003). Samara and Drickamer (1962) demonstrated that the SnS structure was orders of magnitude more electrically resistive than galena at high pressures. We therefore monitored the electrical resistance as a function of pressure along a variety of isotherms to explore the P/T slope of the galena to SnS transition in PbS.

Multianvil Experimental Methods

Our initial reconnaissance in multianvil apparatus was followed by detailed transition reversals in piston/cylinder apparatus. Figure 6 shows the experimental configuration employed for the multianvil experiments. 12 mm truncated edge length (TEL) WC cubes were employed in an 8/6 cylindrical multianvil. A slightly unusual fin-to-fin metal heater geometry facilitated the introduction of resistance and thermocouple leads without the undue complexity of the normal face-to-face geometry of heater. The pressure medium outside the heater was Aremco 584OF castable ceramic (Walker, 1991). Ozark Technical Ceramics grade HP crushable MgO was used within the FeCrAlloy® metal heater as pressure medium and sample container. Chromel-alumel (type K) thermocouple wire formed a junction embedded in one end of a galena cylinder at the hot spot of the furnace. The other end of the galena cylinder has a single alumel wire in contact with it. This wire and the negative lead of the K thermocouple formed the contact wires for the resistance measurement circuit monitored at intervals by an Agilent 34401A multimeter when the thermocouple was disconnected from its measurement and control circuit. The metal heater and power supply were stable enough that, once temperature had been stabilized for a few minutes in feedback control mode, a bumpless transition to power control mode rarely caused drift in temperature greater than 1 °C, at which time the PbS resistance could be measured. Pressures were calibrated against the Bi I-II transition at 25.5 kbar, which was found to occur at 125 tons press force on in-stroke pressurization of the 12 mm TEL assembly.

Our starting material was a cylinder of pressed mm-sized chunks of clean natural galena. The pressure was increased through a region of known galena stability until a transition was noted in the form of a substantial increase in sample resistance at which point the pressure was decreased. The resistance traces with pressure are smooth and well-behaved, unlike those produced from the 200 mesh synthetic 99.9 percent PbS powder used in the melting study. Although the chemical purity of the natural material was undoubtedly less than the synthetic, resistivity is evidently sensitive to other properties that differ across the two starting materials. Resistivity could be affected by grain size or by the possible small amounts of oxidation or other contaminants of the

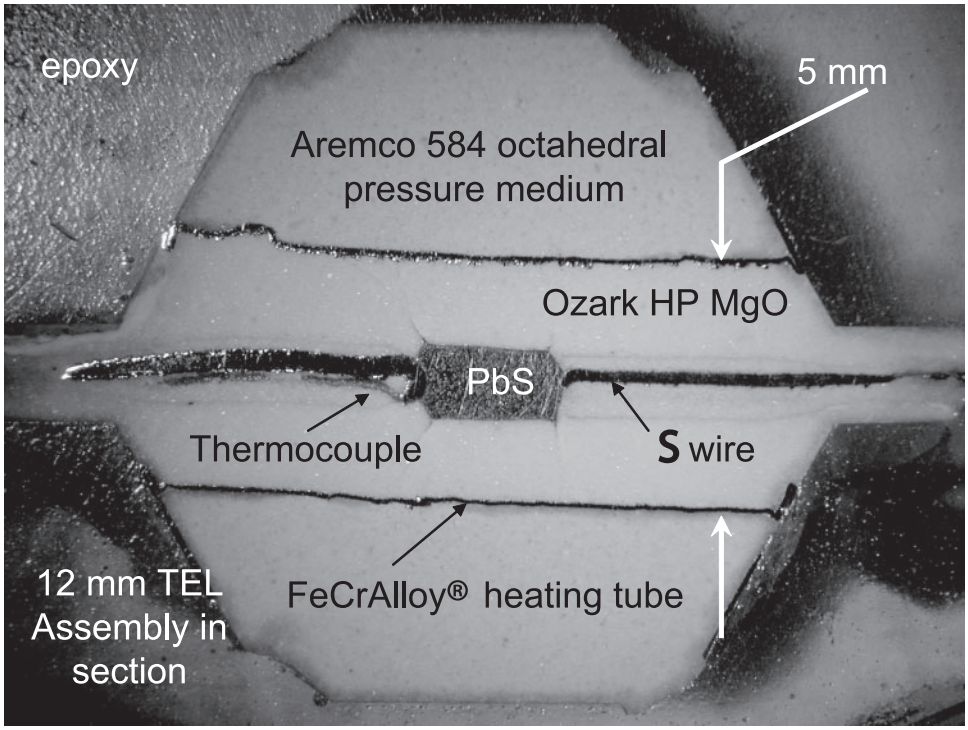

Fig. 6. Section through a compressed multianvil assembly showing thermocouple and resistance wires in contact with PbS cylinder.

synthetic powder residing on the fine particle surfaces. Thus the coarse natural material, in which any contaminants present are not concentrated on grain surfaces and have smaller impact on the resistive properties, served our purpose better than the synthetic material for the resistance measurements.

MULTIANVIL RESULTS—CUBIC GALENA TO ORTHRHOMBIC PbS

Figure 7 shows the resistance traces for three pressure cycles, one at 25 °C, one at 200 °C, and one at 1000 °C. Upon increase of pressure at room temperature, a stepped increase of resistance of several orders of magnitude is observed to begin at ~33 kbar. This increase in resistance ends at about ~52 kbar after which a modest decline in resistance is seen. This step is interpreted as the rock salt to orthorhombic structure transition in PbS. It is considerably smeared in pressure, even when the pressure cycle lasts a day, compared to the sharpness of the Bi calibration trace run in the same assembly in a few hours. The initiation of the transition is at significantly higher pressure than the equilibrium pressure reported for this transition by Bridgman (1940). Upon unloading the pressure, the transition is seen to be reversible. Galena is confirmed as the recovered phase by XRD. A large pressure hysteresis, however, is apparent in the reversibility of the resistance trace. The reverse transformation is only observed to start at a press force that would correspond to about ~23 kbar if it were a compressive stroke. Part of this hysteresis is undoubtedly friction within the multianvil apparatus, as documented by Walker and others (1990) and Walker (1991). The pressure calibrations are only carried out for up-stroke operations. But some of the hysteresis is undoubtedly the MgO pressure medium and especially the PbS itself. Bi

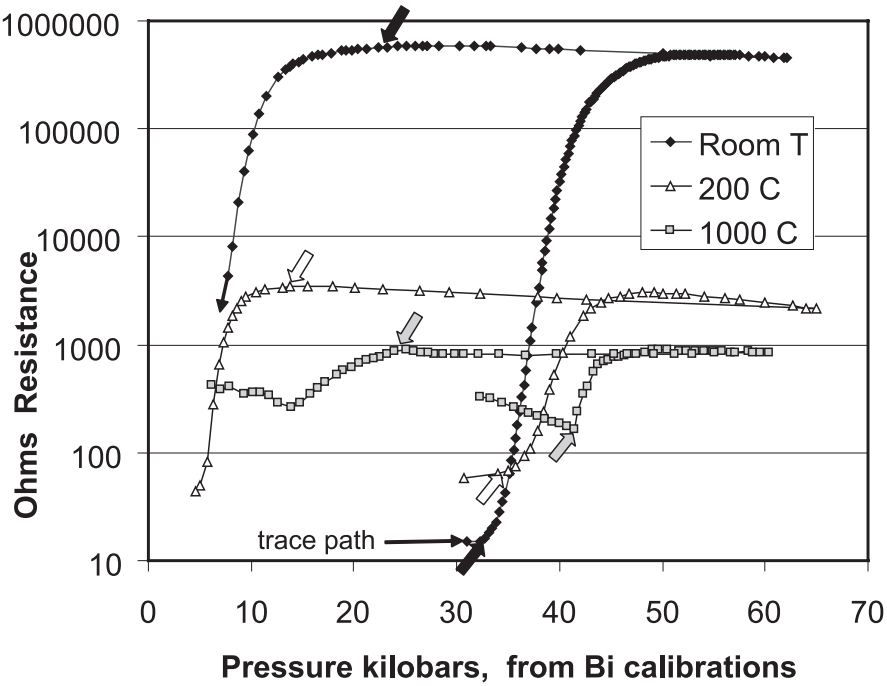

Fig. 7. PbS resistance trace through the galena-SnS transition at three temperatures in octahedral multianvil apparatus with MgO as the pressure medium. Trace begins at the bottom of the right leg of the trace in each experiment and goes to higher pressure until the high resistance of the SnS phase is achieved. Then pressure is unloaded until the low resistance of galena is recovered. Heavy arrows indicate the initiation of the forward transition to SnS on compression and the initiation of the reverse transition to galena on decompression. Wide hysteresis of the transition is seen. Resistance of galena increases with temperature about an order of magnitude in 1000 °C whereas the resistance of SnS-structured PbS drops almost three orders of magnitude in that same temperature interval.

shows much less smearing and hysteresis in its transition behavior in MgO in this device. Bridgman (1940) notes the sluggishness and poor behavior of the galena transition. Our hysteresis envelope does include the ~25 kbar transition pressure previously reported.

We also note that at 1000 °C the transition is still visible by resistive measurement although its character is somewhat different. The onset of the forward and the reverse transitions are more sharply defined, the pressure interval over which the transition occurs is smaller, and the resistance change observed across the transitions is much less. The galena has higher resistance of about an order of magnitude and the SnS-structure has about 3 orders of magnitude lower resistance at 1000 °C than at ambient temperature. These changes in character occur gradually over the 25 to 1000 °C interval. The broadness of the pressure hysteresis loop does not diminish much with temperature; these loops all typically took one working day (~10 hours) to complete. The hysteresis is so broad that a firm conclusion about the precise location of the transition and its P/T slope cannot be drawn from these observations. At best, we conclude that the transition is within the loop, and that the temperature variation is unimpressive. The top of the transition in these rapid multianvil sweeps is out of piston/cylinder pressure range. But if it were indeed at ~ 25 kbar as claimed by previous investigators, then a piston/cylinder investigation of long duration using softer pressure media might be able to define the transition more exactly.

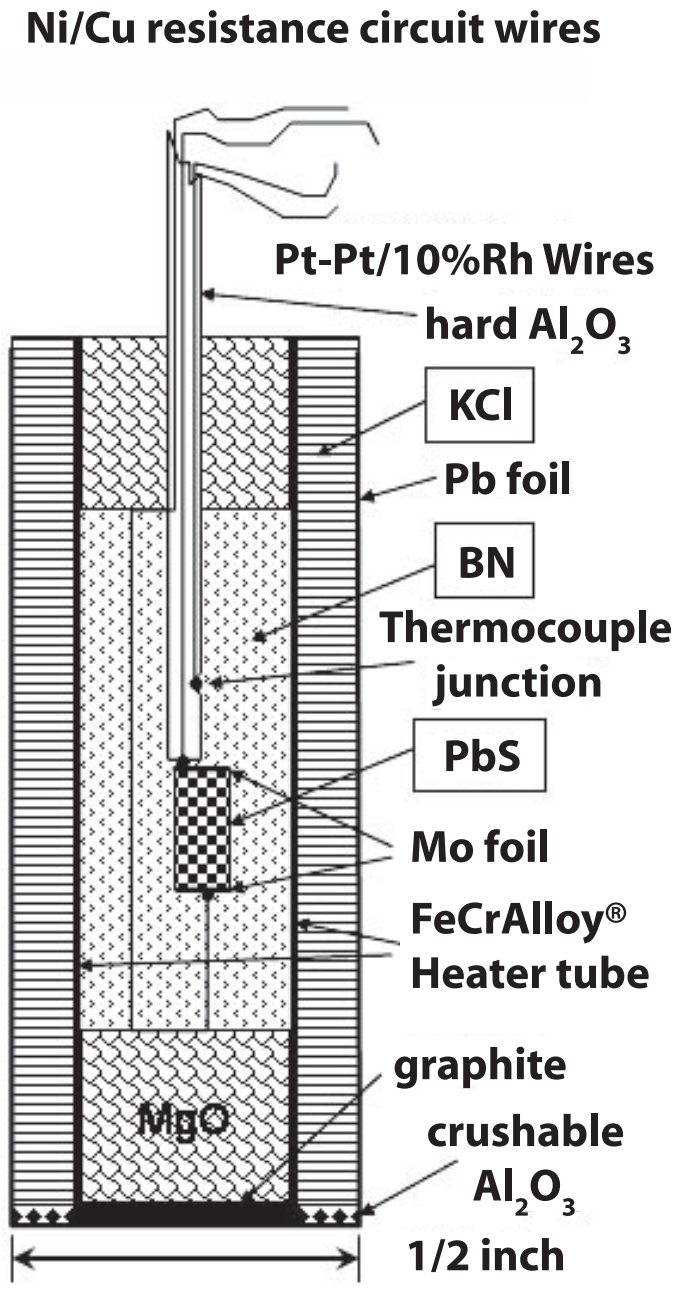

Fig.8. Configuration of piston/cylinder experiments to determine the galena to SnS structure by resistance measurements with reduced pressure hysteresis.

Piston/Cylinder Experimental Methods

Figure 8 shows the combined resistance and temperature circuits employed in a 1/2″ piston/cylinder apparatus of the Boyd-England type. BN was used as a pressure medium immediately around the PbS and its electrical connecting wires. Pt/Pt10Rh

thermocouples (type S), not in contact with the PbS, were used to measure and control temperature. Mo foil caps were put at each end of the PbS cylinder. KCl was used as the pressure medium outside the FeCrAlloy® heater. KCl sylvite, and especially its B2 equivalent encountered at about ~20 kbar, is substantially weaker than MgO or halite (Walker and others, 2002). We expect such a pressure cell to have as little pressure hysteresis as can be practically achieved with solid media. The B1-B2 transition in the pressure medium was visible near 20 kbar as a stasis in the oil pressure during pumping. It was also sometimes visible as a rather bumpy resistance trace through the B1 to B2 transition region. This wrinkle did not interfere with our measurements on PbS whose most interesting region was a few kilobars higher.

Kavner and Walker (2006) employed a 4-wire probe similar to the one used here to make temperature and resistance measurements and to drive redox reactions in metal alloy/silicate electrochemical experiments. In the present case the multimeter was believed not to be driving any electrochemistry. However we did encounter significantly more stray DC and AC mV signals with our BN pressure medium than with MgO in the multianvil configuration seen in figure 6. We suspect that the closeness of the parallel wires in the leads into the probe that enters through imperfectly resistive Al_2O_3 ducting may be instrumental in generating this level of noise. This interference limited our ability to collect transition signals resolvable from noise at temperatures above 600 °C.

piston/cylinder results – cubic to orthorhombic PbS

Figure 9 shows our resistance traces across the transitions at 25 and 600 °C. The piston/cylinder cycles lasting weeks were successfully used to tighten the transition hysteresis loops. We believe that multianvil experiments with similarly weak pressure media might not have been successful on a laboratory time scale because of residual internal friction in the gasketing and slip surfaces between anvils and drivers.

We did not attempt to achieve the plateau on top of the transitions seen in figure 7 as these plateaus might have been out of pressure range. Instead we increased pressure until the resistance change unequivocally indicated that the phase change was underway. Typically this observation would involve increasing the oil pressure and observing the resistance response. If there was no resistance response or if the resistance fell, we concluded we were below the transition and pumped to a higher pressure after a suitable wait, typically a day. However if resistance rose, and specifically if it continued to spontaneously climb as pressure fell back through sample shrinkage and pressure medium compaction, the transition was deemed to be truly underway. During the subsequent unloading part of the pressure cycle, the reverse transition was inferred to be underway if resistance fell spontaneously during pressure unloading. Examples of this behavior are circled in figure 9 for both the up-pressure and down-pressure cycles. At room temperature during a two week pressure cycle, it was possible to tighten the transition bracket to 25.6 ± 0.4 kbar, in agreement with previous investigators. We extend the work of the previous investigators by showing that up to 600 °C, the transition pressure climbs only very slightly, if at all, with temperature to 25.9 ± 0.6 kbar. Figure 9 shows these reversals are achieved with minimal hysteresis of the forward and reverse transitions, in contrast to the experience of figure 7. The KCl cell was a useful remediant to the pressure hysteresis of the transition. The transition is insensitive to temperature. Figure 10 summarizes our observations on the galena to SnS structural transition in PbS.

The information in figure 10 on the inversion of galena to a high pressure structure as a function of temperature requires no departure of the P-T slope from a near-vertical line. However, the data permit a slight decrease of the transition P with increasing T to 400 or 500 °C, followed by a slight increase in P at still higher T. The change in the resistance character of the transition over this T interval is also

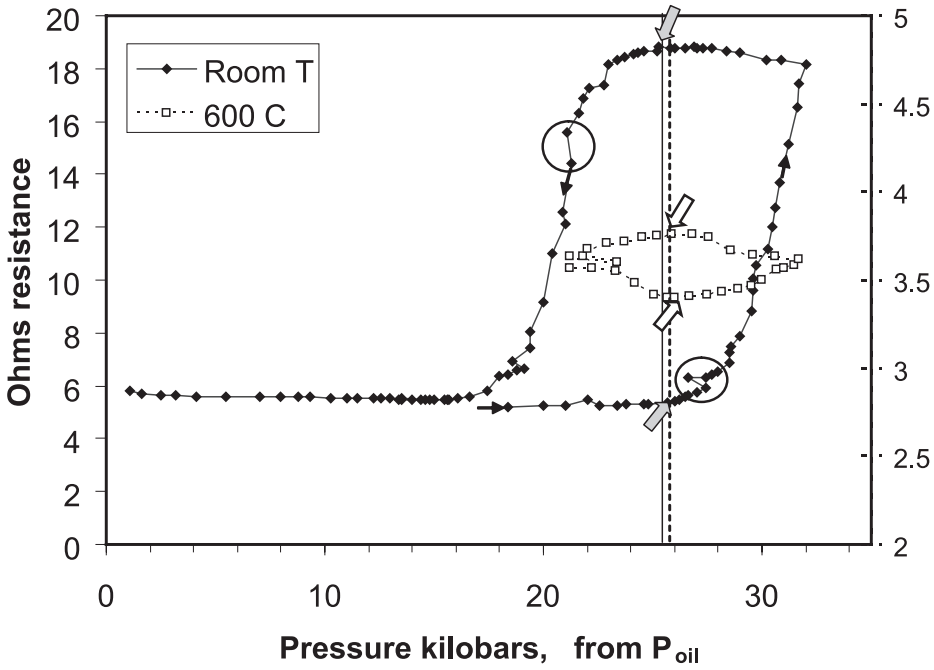

Fig. 9. PbS resistance traces through the galena-SnS transition at two temperatures in piston/cylinder apparatus with BN/KCl as the pressure medium. The room T trace took over 2 weeks to complete. The reversal with limited pressure coverage at 600 °C was achieved in 2 full days. Complete conversion to SnS-structured phase was not attempted. The forward transition was considered initiated by spontaneous resistance climb and the reverse transition was considered initiated with resistance fall on unloading. Circled regions of the room T trace show relaxation modes clearly indicating that the transition has been passed. For instance on the compression stroke, relaxation leads to spontaneous resistance increase rather than decrease. The thick arrows, pointing to the initiation of the galena to SnS phase up-pressure and the reversal down-pressure, indicate that there is very little hysteresis in this assembly and that the transition is rather close to 26 kbar at all temperatures studied. This result does not contradict the results from multianvil experiments. It simply illuminates results that were not visible because of the poorer pressure resolution of the multianvil transitions. Both transition sluggishness and stiffness of the pressure medium contributed to that poor resolution. The sluggishness was evaded here by performing slow traces in soft pressure media.

permissive of such an interpretation, but by no means requires it. An additional phase transition within crystalline PbS to a higher-entropy form than galena, within a wedge of P-T space extending to higher T and lower P from ~500 °C and 25 kbar, may be indicated. No transitions are known within galena with increasing T to the melting point at low P, so the wedge does not extend to 1 bar. PbS melting experiments at elevated P recover galena, so this additional phase, if it exists, is not quenchable. Herzenbergite, SnS in the α-SnS structure, is known to have an unquenchable high-temperature polymorph, β-SnS (Robie and others, 1979). Thus an additional P-T field of yet another PbS polymorph beyond galena and α-SnS-like is not unimaginable. We cannot address this possibility further with present data; *in situ* XRD would be required for resolution of whether or not another unquenchable polymorph exists, and whether it has β-SnS structure, or still another form. Whatever the resolution may be, it has little impact on our conclusion that the transition from galena-like PbS to α-SnS-like PbS does not have much variation of P as T increases, and that the transition intersects the liquidus at an opportune pressure to explain the liquidus flattening into the transition pressure of ~26 kbar.

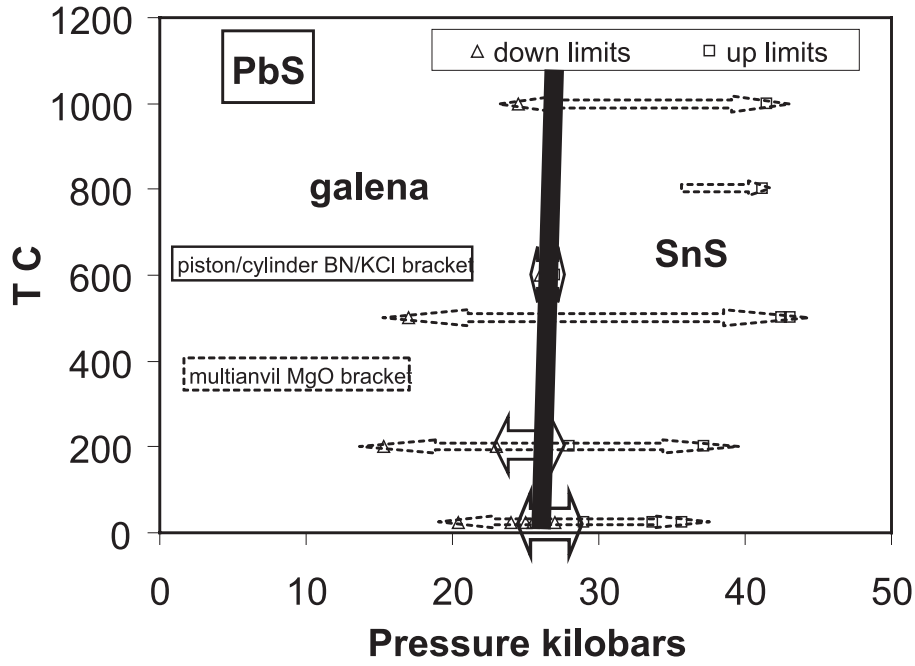

Fig. 10. Summary of the brackets on the transition from galena to SnS structure in PbS. The transition occurs at 26 kbar, more or less independent of temperature.

DISCUSSION OF PHASE BOUNDARY SLOPES

Liquidus

We compare galena's melting behavior with the liquidi of other similarly sized and structured compounds. Figure 11 shows the melting curves of FeS and several cubic NaCl-structured (B1) compounds with unit cells similar in size to galena. The liquids slopes and shapes vary significantly. Galena's initial liquidus slope at 14.4 °C/kbar is less than KCl (18.3) and NaBr (22.9), but more than AgCl (9.6) and AgBr(11.6) (table 2). The curvature is greater for PbS, KCl and NaBr than it is for AgCl and AgBr. PbS and KCl both have phase transitions within the pressure range of the plot while the other compounds do not. This section will discuss potential influences on the systematic variation of these liquidus slopes and curvatures.

Liquidus slopes follow from volume and entropy changes upon melting through the Clausius-Clapeyron equation:

$$dT_m/dP = \Delta V_m/\Delta S_m.$$

Indeed, the measured initial liquidus slopes from this study and others increase linearly with increasing literature values for one atmosphere melting volume, consistent with Clapeyron behavior and simple $\triangle S_m$ (fig. 12, table 2). In this context 'simple' $\triangle S_m$ is taken to mean that $\triangle S_m$ is either ~constant or linearly related to $\triangle V_m$. The fit is best for lower-slope liquidii, but is still within the wider error bars of the higher-slope compounds.

In contrast, the $\triangle S_m$s are known for these compounds and they are anything but simply behaved. Figure 13 plots $\triangle V_m/(dT_m/dP)$ against literature values of $\triangle S_m$. Ideally, $\triangle V_m/(dT_m/dP)$ should equal $\triangle S_m$,forming a straight line passing through the

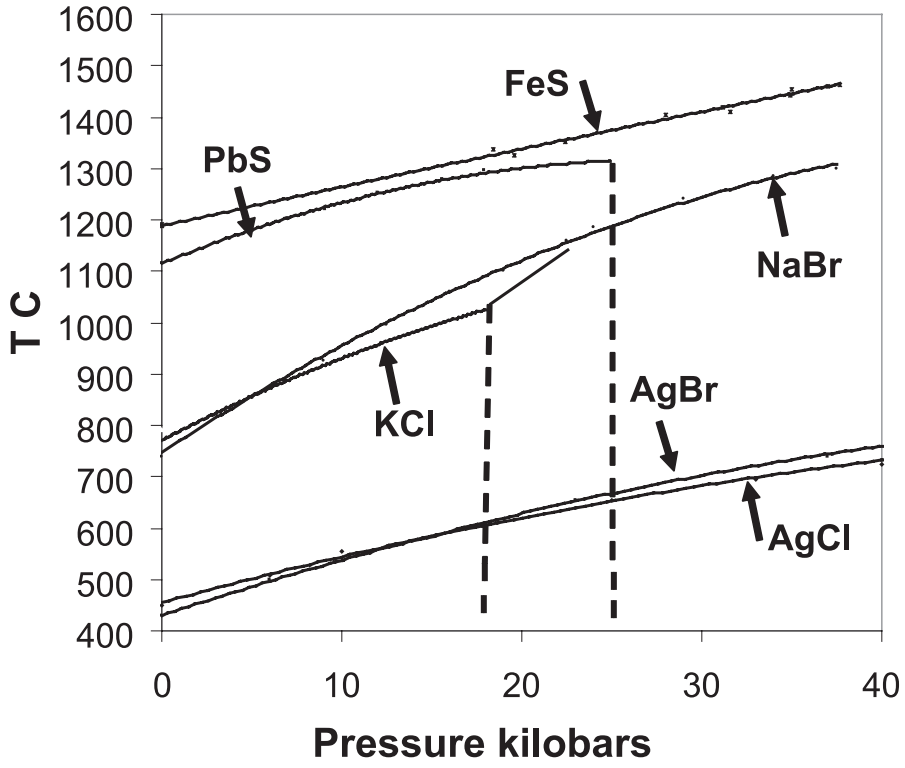

Fig. 11. Plot of experimentally determined liquidi for PbS, other similarly sized and structured compounds and FeS. PbS data are from this study. FeS from Ryzhenko and Kennedy, 1973; NaBr: Pistorius, 1966; KCl: Clark, 1959; AgBr and AgCl: Akella and others, 1969.

origin with a slope of one. Instead, the points form two lines both with negative slopes. PbS, FeS, AgBr and AgCl plot together along one line while NaBr and KCl form a separate parallel line. The significance of these two lines, if one even exists, is not immediately apparent to us. Furthermore, most compounds lie to the left of the 1:1 line indicating either systematic underestimation of $\triangle S_m$ or overestimation of $\triangle V_m$. The previous work of Clark (1959) reports similar observations for several ionic salts. Like Clark, assuming the measured liquidus slopes and compositions are correct, we conclude that the discrepancy stems from either erroneous $\triangle S_m$ or $\triangle V_m$ values. We suspect underestimation of $\triangle S_m$s because of the good relationship between $\triangle V_m$ and (dT_m/dP) displayed in figure 12. If this explanation is correct, the literature value for the $\triangle S_m$ of PbS is underestimated by approximately 100 percent. A discrepancy of this magnitude is rightly the cause of some anxiety. One possible resolution might be via small departures from stoichiometery as suggested by Bloem and Kröger (1956). Such departures could stem from either original non-stoichiometry in the starting material or from preferential loss of either Pb or S. It is difficult, however, to imagine that miniscule (sub-detection level) departures from stoichiometry permitted within the error of our measurements could introduce such large entropy effects. Even a 10 percent compositional error would yield only ~3 J/mol*K in entropy difference, only ~25 percent of that needed to explain the observed entropy difference.

Non-unary melting of PbS at high pressure has been suggested as another source for our entropy discrepancy. The development of incongruent melting behavior at

TABLE 2

Thermodynamic and compressibility values

Compound	Initial Slope K/kbar	Initial Curvature $K^2/kbar^2$	V Solid cm^3/mol	V Liq. cm^3/mol	ΔV_m cm^3/mol	S Solid J/mol*K	S Liquid J/mol* K	ΔS_m J/mol*K	Comp. Solid $10^{-12}*cm^2/dyne$	Comp. Liq. $10^{-12}*cm^2/dyne$	Ref
PbS	14.4	-0.5132	33.03	36.60	3.58	173.36	186.93	13.57	1.5	~12*	1,2,3,4
AgCl	9.6	-0.1322	27.30	29.42	2.12	148.97	166.67	17.70	2.3	8.5	2,3,5,6,7
AgBr	11.6	-0.168	30.54	33.65	3.11	162.63	175.66	13.03	2.5	9.7	2,3,5,6,7
KCl	18.3	-0.4568	42.82	48.82	7.00	153.95	179.15	25.20	5.6	38.4	2,3,5,8
NaBr	22.9	-0.4226	36.23	43.94	7.71	155.45	181.04	25.59	5.0	33.6	2,3,5,9
FeS	7.7	-0.0184	21.09	22.54	1.447	168.30	190.33	22.03	1.22	12.5	3,10,11,12

[1]Fei (1995), [2]Janz (1967), [3]Robie and others (1979), [4]Knoor and others (2003), [5]Touloukian and others (1977), [6]Loje and Schuele (1970), [7]Takesawa and others (1989), [8]Walker and others (2002), [9]He and Yan (2001), [10]Barthelmy (2006), [11]Sanloup and others (2000), [12]King and Prewitt (1982), *prospective

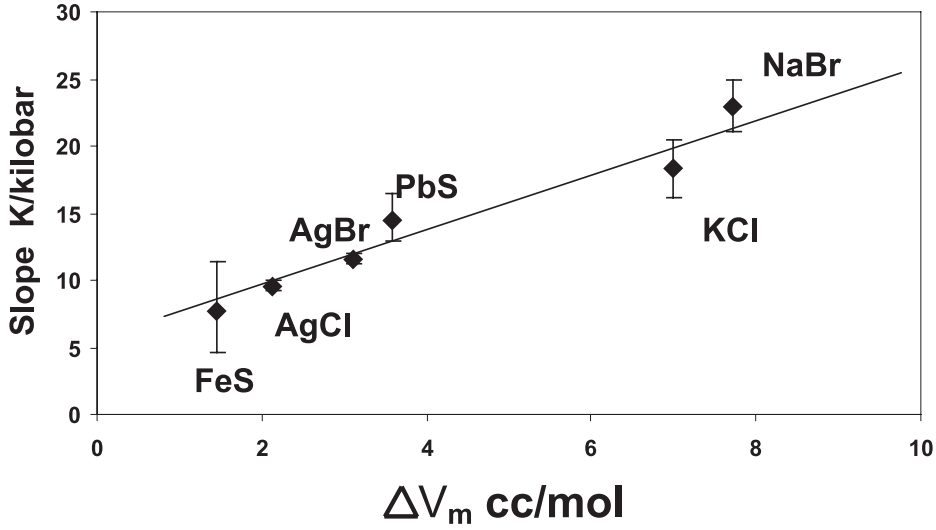

Fig. 12. Plot of liquidus slopes against $\triangle V_m$ for compounds analogous to PbS. Data suggest that $\triangle V_m$ influences melting slope.

pressure would explain the weakened melting signal and could even cause the liquidus to flatten. We contend, however, that non-unary melting encountered at pressure would have diminished impact on our one-atmosphere entropy values, which are calculated with initial liquidus slopes that respond only weakly to the high-pressure region of the liquidus. Furthermore, non-unary melting at one atmosphere fails to dispel the discrepancy between the entropy values calculated from the liquidus and those measured directly. Thus, with neither non-stoichiometry nor incongruent melting to explain the observed entropy discrepancies, we are left with the choice between suspending belief in either the Clausius-Clapeyron formulation or the $\triangle S_m$ data. We have sensibly chosen to suspect the latter.

As mentioned above, in addition to differences in initial slopes, the liquidi in figure 11 differ in curvature (table 2). Curvature in these liquidii can be largely explained by the ratio of liquid to solid compressibilities at one atmosphere (fig. 14). AgCl, AgBr, NaBr and KCl lie along a linear trend that almost includes FeS. [FeS may in reality lie closer as its liquid state compressibility was measured at ~200°C above the liquidus and its solid compressibility at room temperature. Furthermore FeS is not B1-structured.] Greater liquid/solid compressibility causes greater curvature because the liquid phase progressively stabilizes at higher pressure and lower temperatures than might be expected through linear extrapolation of lower pressure results. The more compressible liquid undergoes more of a volume reduction and therefore finds its phase stability volume to decrease less rapidly than it otherwise might with increasing pressure at the expense of the denser, less-compressible solid. PbS is plotted prospectively in figure 14 because, as far we know, its liquid compressibility is not yet published. If PbS obeys the same compressibility-curvature relationship, its liquid compressibility should be on the order of $12*10^{-12}$ cm^2/ dyne (bulk modulus ~8.3 GPa), more compressible than even KCl.

The strong relationship between halide liquidus curvatures and compressibility ratios seen in figure 14 further reduces the need to invoke non-unary melting in PbS to explain PbS liquidus flattening at high pressure that is complementary to the observed freezing signal weakness. The decrease in liquidus slope for PbS and for most of the

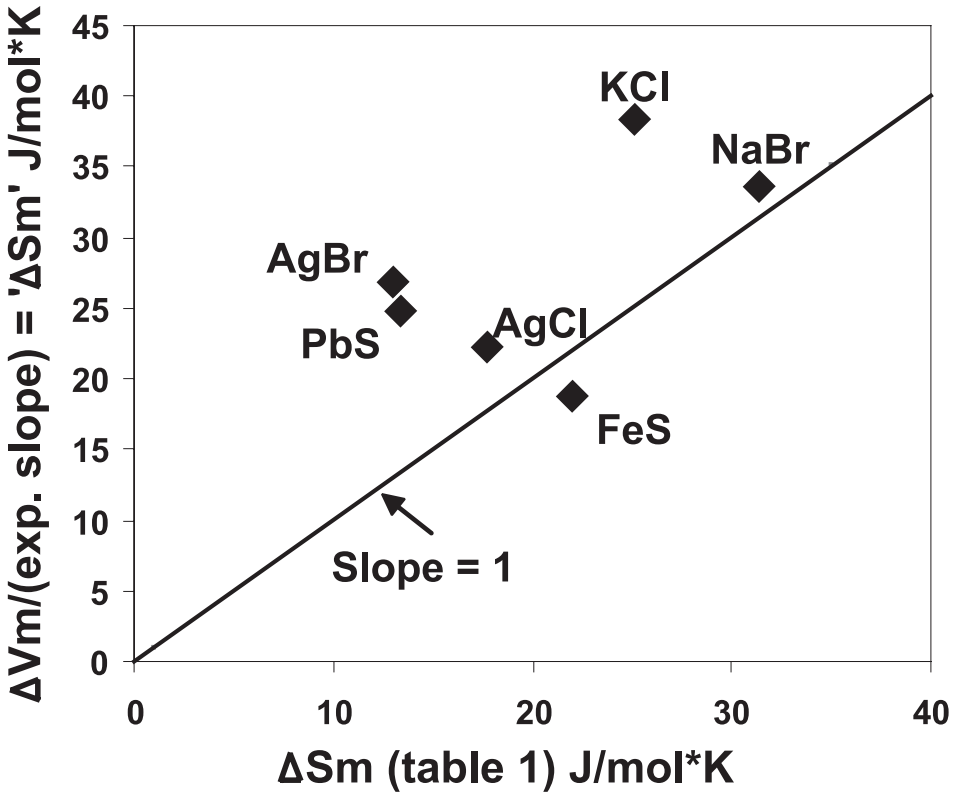

Fig. 13. Literature $\triangle S_m$ values differ significantly from values calculated with $\triangle V_m$, and initial liquidus slope via the Clapeyron equation. Most literature values are found to the left of the 1:1 correlation line indicating either erroneously small literature $\triangle S_m$ values, systematically erroneous volume measurements, incorrect initial liquidus slopes determination, or a combination of the three. Given our confidence in liquidus slope and volume measurements, we strongly suspect the literature $\triangle S_m$ values are in error.

other materials surveyed in this study can be explained by solid/liquid compressibility differences obviating the need to invoke non-unary melting as a special exception for PbS.

Cubic to Orthorhombic Phase Transition

The cubic galena to orthorhombic transition does have a steep enough P-T trajectory to bring it to the liquidus in a position to plausibly explain the flattening of the PbS liquidus. The explanation is that the densification of the solid phases occurs discontinuously across a heterogeneous equilibrium between two crystalline polymorphs. At higher temperatures, however, the analogous densification occurs continuously as a homogeneous equilibrium within the liquid phase. A mix will always exist of higher and lower density species in the liquid that shifts continuously in favor of the high density forms at high pressure. Therefore some dense species occur in the liquid at pressures below the solid state transition and these species increase in proportion as the pressure increases. Thus ΔV of the Clapeyron slope of the melting equilibrium decreases with pressure, and the liquidus "droops" approaching the transition pressure. The remarkable insensitivity of the galena-SnS-like transition to temperature indicates that ΔS has nearly vanished. This vanishing leads to the expectation that the liquid-state species transitions are also largely pressure-driven; the only role for entropy

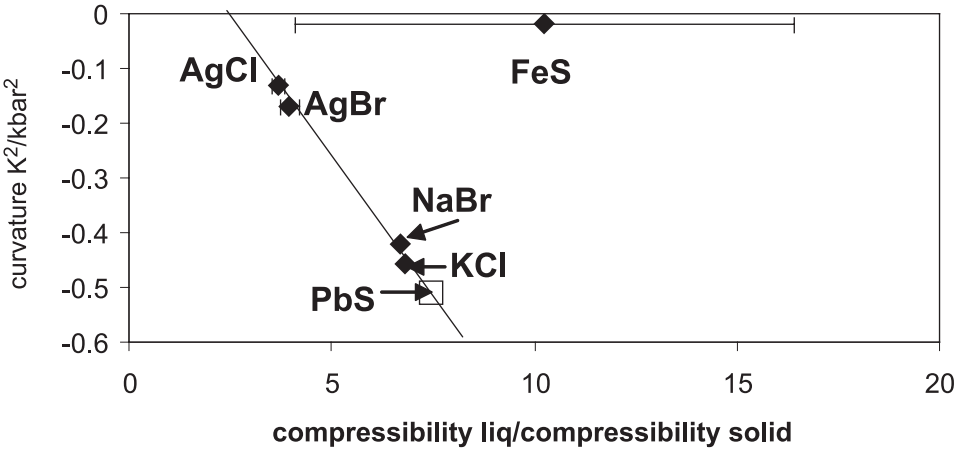

Fig. 14. Plot of curvature against solid/liquid compressibility ratio for PbS and analogous compounds. Most data plot along a single line. Provided PbS abides by the same systematics, it would have a compressibility ratio of approximately 7.5 and a compressibility of approximately $12*10^{-12}$ cm^2/ dyne (bulk modulus ~8.3 GPa) (open square).

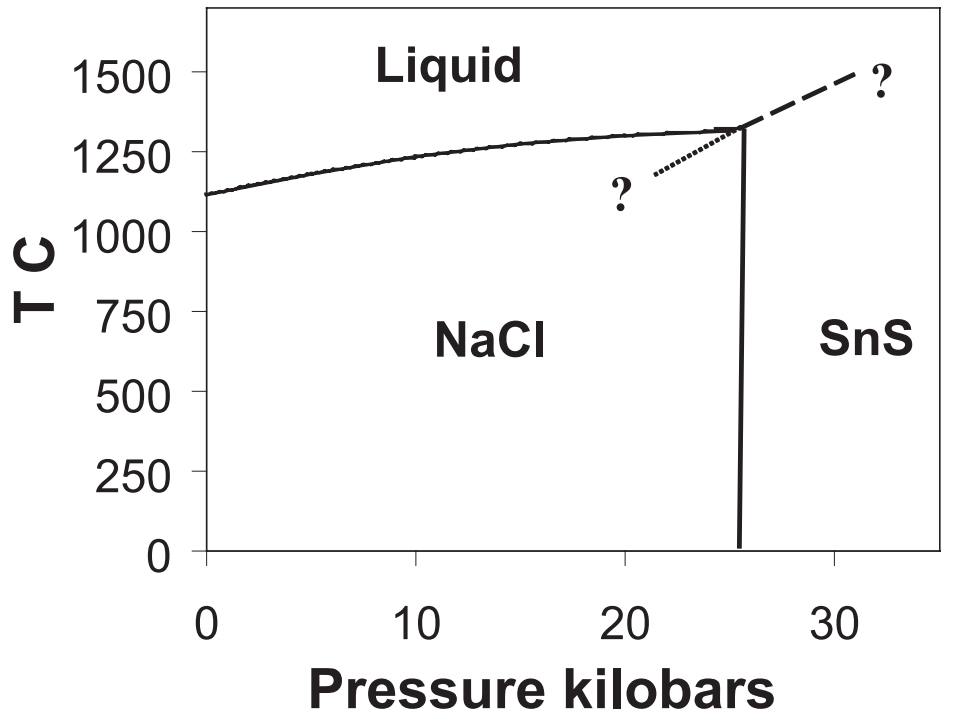

Fig. 15. Summary of galena stability which is terminated by melting at high temperature and by inversion to SnS-like structure at 26 kbar. The triple point between galena, liquid, and SnS-structured PbS is inferred to be at 1315 °C and 26 kbar.

is to stabilize the mixture of species over a range of pressures. The minimal role of entropy in similar solid-state densification transitions is also seen in the vertical slopes of the transitions between the K alkali halides reported by Pistorious (1965). This observation is reassuring, given the similarity of structures to PbS.

CONCLUSION

PbS's phase relations up to 26 kbar are summarized in figure 15. The liquidus of galena increases from 1191°C at 5.9 kbar to 1315°C at ~25 kbar along a curve of decreasing slope that cannot be accurately described with the Clausius-Clapeyron equation and literature entropy values. However, systematic variation in liquidus curvature with melt/solid compressibility ratio allows an estimation of PbS liquid bulk modulus of ~8 GPa. The transition of galena to the SnS-like structure is found to occur at ~26 kbar regardless of temperature, giving an inferred triple point at ~26 kbar and 1315 °C shown in figure 15. The curvature of the galena liquidus reflects the approach to this triple point as the structure in the liquid state previews the solid-state transition.

ACKNOWLEDGMENTS

This work was supported by the US National Science Foundation. We thank Richard Sack and an anonymous reviewer for their insightful and helpful comments. LDEO contribution 7033.

REFERENCES

Akella, J. C., and Kennedy, G. C., 1971, Melting of gold, silver, and copper—proposal for a new high-pressure calibration scale: Journal of Geophysical Research, v. 79, p. 4969–4977.

Akella, J., Vaidya, S. N., and Kennedy, G. C., 1969, Melting of silver halides at high pressure: Journal of Applied Physics, v. 40, p. 2800–2805.

Barthelmy, D., May 2006, Webmineral, 14 May 2006. http://webmineral.com/

Blitz, W., 1908, Notizen über schmelzen und sublimieren einiger sulfide: Zeitschrift für Anorganische Chemie, v. 59, p. 273–284.

Bloem, J., and Kröger, F. A., 1956, The p-T-x phase diagram of the lead-sulfur system: Zeitschrift für Physikalische, neue folge, v. 7, p. 1–14.

Boehler, R., 1992, Melting of the Fe-FeO and the Fe-FeS systems at high pressure: constraints on core temperatures: Earth and Planetary Science Letters, v. 111, p. 217–227.

Brigman, P. W., 1940, The compression of 46 substances to 50,000 kg/cm^3: Proceeding of the American Academy of Arts and Sciences, v. 74, p. 21–51.

Chattopadhyay, T., von Schnering, H. G., Grosshans, W. A., and Holzapfel, W. B., 1986, High pressure X-ray diffraction study on the structural phase transitions in PbS, PbSe and PbTe with synchrotron radiation: Physica B, v. 139 and 140, p. 356–360.

Clark, S. P., 1959, Effect of pressure on the melting points of eight alkali halides: The Journal of Chemical Physics, v. 31, p. 1526–1531.

Donnay, J. D. H., and Ondik, H. M., 1973, Crystal data: Determinative tables, *in* Inorganic compounds: U.S. Department of Commerce, National Bureau of Standards and Joint Committee on Powder Diffraction Standards. Third Edition, Vol. II.

Fei, Y., 1995, Thermal expansion, *in* Ahrens, T., editor, Mineral Physics and Crystallography – a handbook of physical constants: AGU Reference Shelf, v. 2, p. 283–291.

Fram, M., and Longhi, J., 1992, Phase equilibria of dikes associated with Proterozoic anorthosite complexes: American Mineralogist, v. 77, p. 605–616.

Friedrich, K., 1907a, Die Schmelzdiagramme der binären systeme bleiglanz-magnetkies und bleiglanz-schwefelsilber: Metallurgie, v. 4, p. 479–485.

——— 1907b, Die Schmelzdiagramme der binären systeme schwefelsilber-kupfersulfür und bleiglanz-kupfersulfür: Metallurgie, v. 4, p. 671–673.

Friedrich, K., and Leroux, A., 1905, Blei und Schwefel: Metallurgie, v. 2, p. 536–539.

He, Q., and Yan, Z., 2001, Study of temperature dependence of bulk modulus and interatomic separation for ionic solids: Physica Status Solidi, v. 223, p. 767–771.

Heike, W., 1912, Zinnhaltiger bleiglanz aus einem eisenhochofen und das system schwefelblei und schwefelzinn: Metallurgie, v. 9, p. 313–319.

Janz, G., 1967, Molten Salts Handbook: New York, Academic Press, 184 p.

Jeanloz, R., and Roufosse, M., 1982, Anharmonic properties: ionic model of the effects of compression and coordination change: Journal of Geophysical Research, v. 87, p. 10,764–10772

Kavner, A., and Walker, D., 2006, Core/mantle-like interactions in an electric field: Earth and Planetary Science Letters, v. 248, p. 316–329.

Kavner, A., Duffy, T. S., and Shen, S., 2001, Phase stability and density of FeS at high pressures and temperatures: implications for the interior structure of Mars: Earth and Planetary Science Letters, v. 185, p. 25–33.
King, E., and Prewitt, C., 1982, High-pressure and high-temperature polymorphism of iron sulfide (FeS): Acta Crystallographica, v. B38, p. 1877–1887.
Knoor, K., Ehm, L., Hytha, M., Winkler, B., and Depmeier, W., 2003, The high-pressure α/β phase transition in lead sulfide (PbS) X-ray powder diffraction and quantum mechanical calculations: European Physical Journal B, v. 31, p. 297–303.
Kullerud, G., 1969, The lead-sulfur system: American Journal of Science, v. 267-A, p. 233–256.
Loje, K., and Schuele, D., 1970, The pressure and temperature derivatives of the elastic constants of AgBr and AgCl: Journal of Physics and Chemistry of Solids, v. 31, p. 2051–2067.
Mariano, A. N., and Chopra, K. L., 1967, Polymorphism in some 4-6 compounds induced by high pressure and thin-film epitaxial growth: Applied Physics Letters, v. 10, p. 282–284.
Pistorius, C.W.F.T., 1966, Effect of pressure on melting points of sodium halides: Journal of Chemical Physics, v. 45, p. 3513–3519.
Robie, R. A., Hemingway, B. S., and Fisher, J. R., 1979, Thermodynamic properties of minerals and related substances at 298.15 K and 1 bar (10^5 pascals) pressure and at higher temperatures: U.S. Geological Survey Bulletin 1452 reprinted with corrections, 456 p.
Ryzhenko, B., and Kennedy, G. C., 1973, The effect of pressure on the eutectic of the system Fe-FeS: American Journal of Science, v. 273, p. 803–810.
Samara, G. A., and Drickamer, H. G., 1962, Effect of pressure on resistance of PbS and PbTe: Journal of Chemical Physics, v. 37, p. 1159.
Sanloup, C., Guyot, F., Gillet, P., Fiquet, G., Mezouar, M., and Martinez, I., 2000, Density measurements of liquid Fe-S alloys at high-pressure: Geophysical Research Letters, v. 27, p. 811–814.
Sharp, W. E., 1969, Melting curves of sphalerite, galena, and pyrrhotite and the decomposition curve of pyrite between 30 and 65 kilobars: Journal of Geophysical Research, v. 74, p. 1645–1652.
Takahashi, T., Bassett W. A., and Weaver, J. S., 1964, Crystallographic study of high-pressure lead sulfide, selenide, and telluride, and its implication to the study of the mantle: Geologial Society of America Special Papers, v. 76, p. 162–163.
Takesawa, K., Takeda, S., Harada, S., and Tamaki, S., 1989, Sound wave propagation in molten silver halides: Journal of the Physical Society of Japan, v. 58, p. 538–543.
Touloukian, Y., Kirby, R., Taylor R., and Lee, T., 1977, Thermal Expansion *from* Thermophysical properties of matter: New York, IFI/Plenum, v. 13, 1658 p.
Truthe, W., 1912, Über das verhalten der sulfide von Pb, Cu, Ag, und des Cu_2O in den schmelzen der zugerhörigen chloride: Zeitschrift für Anorganische Chemie, v. 76, p. 161–173.
Van Hook, H. J., 1960, The ternary system Ag_2S-Bi_2S_3-PbS: Economic Geology, v. 55, p. 759–788.
Wakabayashi, I., Kobayashi, H., Nagasaki, H., and Minomura, S., 1968, The effect of pressure on the lattice parameters: Part I. PbS and PbTe, Part II. Gd, NiO, and α-MnS: Journal of the Physical Society of Japan, v. 25, p. 227–233.
Walker, D., 1991, Lubrication, gasketing, and precision in multianvil experiments: American Mineralogist, v. 76, p. 1092–1100.
Walker, D., Carpenter, M. A., and Hitch, C. M., 1990, Some simplifications to multianvil devices for high pressure experiments: American Mineralogist, v. 75, p. 1020–1028.
Walker D., Cranswick, L. M. D., Verma, P. K., Clark, S. M., and Buhre, S., 2002, Thermal equations of state for B1 and B2 KCl: American Mineralogist, v. 87, p. 805–812.
Williams, Q., and Jeanloz, R., 1990, Melting relations in the iron-sulfur system at ultra-high pressures: implications for the thermal state of the earth: Journal of Geophysical Research, v. 95, p. 19299–19310.
Winter, M., April 2006, Webelement: U. of Sheffield and Webelements Ltd. 28 April 2006. http://www.webelements.communicate/.